

$\Lambda\bar{\Lambda}$ final-state interaction in the reactions $e^+e^- \rightarrow \phi\Lambda\bar{\Lambda}$ and $e^+e^- \rightarrow \eta\Lambda\bar{\Lambda}$

Johann Haidenbauer^{1,a}, Ulf-G. Meißner^{2,1,b}

¹Institute for Advanced Simulation (IAS-4), Institut für Kernphysik (IKP-3) and Jülich Center for Hadron Physics, Forschungszentrum Jülich, D-52428 Jülich, Germany

²Helmholtz-Institut für Strahlen- und Kernphysik and Bethe Center for Theoretical Physics, Universität Bonn, D-53115 Bonn, Germany

March 10, 2023

Abstract Near-threshold $\Lambda\bar{\Lambda}$ mass spectra for the reactions $e^+e^- \rightarrow \eta\Lambda\bar{\Lambda}$ and $e^+e^- \rightarrow \phi\Lambda\bar{\Lambda}$ are investigated with an emphasis on the role played by the interaction in the $\Lambda\bar{\Lambda}$ system. A variety of $\Lambda\bar{\Lambda}$ potential models is employed that have been established in the analysis of data on $p\bar{p} \rightarrow \Lambda\bar{\Lambda}$ in the past. It is shown that the near-threshold enhancement observed for the two e^+e^- reactions can be reproduced by considering the $\Lambda\bar{\Lambda}$ final-state interaction in the partial waves suggested by the helicity-angle analysis of the experiments. For $e^+e^- \rightarrow \eta\Lambda\bar{\Lambda}$ the same $\Lambda\bar{\Lambda}$ S -wave interaction as in $e^+e^- \rightarrow \Lambda\bar{\Lambda}$ is relevant and with it a consistent description of the pertinent measurements can be achieved. It is pointed out that a nonzero threshold cross section as observed for the latter reaction is not supported by the new $\eta\Lambda\bar{\Lambda}$ data.

Keywords Hadron production in e^+e^- interactions · $\Lambda\bar{\Lambda}$ interaction

PACS 13.60.Rj · 13.66.Bc · 14.20.Jn

1 Introduction

Experimental information on the properties of baryon-antibaryon ($B\bar{B}$) interactions is rather scarce, with the exception of the $N\bar{N}$ system, of course, where standard scattering experiments are possible [1]. For others, like those involving strange baryons and/or antibaryons, constraints on the forces can be only inferred from studies of reactions where the $B\bar{B}$ state is produced and interacts in the final state. Here, the by far best investigated system is $\Lambda\bar{\Lambda}$. In particular, the hyperon production process $p\bar{p} \rightarrow \Lambda\bar{\Lambda}$ has been exten-

sively measured in the PS185 experiment at the LEAR facility at CERN and data are available for total and differential cross sections, but also for spin-dependent observables [1–6], owing to the fact that one can exploit the self-analyzing weak Λ decay. These data span the energy range from the reaction threshold up to $\sqrt{s} \approx 2.4$ GeV.

In the last two decades several other reactions producing a $\Lambda\bar{\Lambda}$ pair have been studied experimentally. Among them are the decays $B \rightarrow K\Lambda\bar{\Lambda}$ [7], $B \rightarrow D\Lambda\bar{\Lambda}$ [8], $J/\psi, \psi(3868) \rightarrow \eta\Lambda\bar{\Lambda}, \pi^0\Lambda\bar{\Lambda}$ [9, 10], and $\psi(3868) \rightarrow \omega\Lambda\bar{\Lambda}$ [11]. In addition, data for $e^+e^- \rightarrow \Lambda\bar{\Lambda}$ [12–17], and for $e^+e^- \rightarrow \phi\Lambda\bar{\Lambda}$ [18] and $e^+e^- \rightarrow \eta\Lambda\bar{\Lambda}$ [19] have been presented. Furthermore, there have been measurements of $\Lambda\bar{\Lambda}$ correlation functions in heavy-ion collisions and in high energy pp collisions by the ALICE Collaboration [20, 21]. Finally, there are preliminary results from GlueX for $\gamma p \rightarrow p\Lambda\bar{\Lambda}$ [22, 23]. See also the recent reviews [24, 25].

Among those reactions, the one that received the by far strongest attention by theorists is $e^+e^- \rightarrow \Lambda\bar{\Lambda}$, since it allows one to determine the electromagnetic form factors of the Λ in the time-like region [26–38]. One-photon exchange can be expected to dominate, so that the reaction mechanism is practically known, and the partial waves of the final state are restricted to either 3S_1 or 3D_1 . Certainly the most conspicuous aspect was the observation of a large non-zero cross section barely 1 MeV away from the $\Lambda\bar{\Lambda}$ threshold in the BES-III experiment [15]. While the near-threshold energy dependence of the reaction cross section reported by the BaBar collaboration [13] could be well described by assuming a standard final-state interaction (FSI) between the $\Lambda\bar{\Lambda}$ pair [28], the explanation of the very large “at threshold” BESIII value required the inclusion of a so far unobserved narrow resonance [30, 35].

^ae-mail: j.haidenbauer@fz-juelich.de

^be-mail: meissner@hiskp.uni-bonn.de

Table 1 Allowed $\Lambda\bar{\Lambda}$ partial waves and J^{PC} assignments (up to P -waves) for various channels in the reaction $e^+e^- \rightarrow \gamma \rightarrow X$.

final state	partial waves
$\phi\Lambda\bar{\Lambda}$	$^1S_0 [0^{-+}], ^3P_0 [0^{++}], ^3P_1 [1^{++}], ^3P_2 [2^{++}]$
$\eta\Lambda\bar{\Lambda}$	$^3S_1 [1^{--}], ^1P_1 [1^{+-}]$
$\Lambda\bar{\Lambda}$	$^3S_1 [1^{--}]$

In the present work we re-investigate the FSI effects caused by the $\Lambda\bar{\Lambda}$ interaction. This is done in view of the new precise measurements of the near-threshold $\Lambda\bar{\Lambda}$ invariant-mass spectrum by BESIII in the reactions $e^+e^- \rightarrow \phi\Lambda\bar{\Lambda}$ [18] and $e^+e^- \rightarrow \eta\Lambda\bar{\Lambda}$ [19]. The former process allows to examine the $\Lambda\bar{\Lambda}$ interaction in other partial waves than in $e^+e^- \rightarrow \Lambda\bar{\Lambda}$, see the selection rules summarized in Table 1, while the latter involves the same final state (3S_1) so that one can explore whether the $\Lambda\bar{\Lambda}$ FSI which describes the energy dependence of the $e^+e^- \rightarrow \Lambda\bar{\Lambda}$ cross section can also explain the one in $e^+e^- \rightarrow \eta\Lambda\bar{\Lambda}$. In particular, it will be interesting to see whether the narrow structure required to describe the BESIII measurement of $e^+e^- \rightarrow \Lambda\bar{\Lambda}$ [30, 35] is also needed in and/or supported by the $e^+e^- \rightarrow \eta\Lambda\bar{\Lambda}$ data.

As in our study of the reaction $e^+e^- \rightarrow \Lambda\bar{\Lambda}$ [28] we employ phenomenological $\Lambda\bar{\Lambda}$ models that have been developed by the Jülich group for the analysis of $p\bar{p} \rightarrow \Lambda\bar{\Lambda}$ data in the past [39–42]. Indeed, in those studies several variants have been established which all describe the PS185 data quite well. These variants have been already used by us for calculating the $e^+e^- \rightarrow \Lambda\bar{\Lambda}$ reaction and yielded cross sections well in line with the BaBar data. Moreover, it turned out that some of the interactions also reproduce roughly the BESIII result [16] on the ratio and phase of the electromagnetic form factors G_E and G_M at 2.396 GeV [34].

The paper is structured in the following way. In the subsequent section we provide a brief overview of the employed formalism for treating the FSI effects. In Sect. 3 we present our results. Specifically, we review the situation for $e^+e^- \rightarrow \Lambda\bar{\Lambda}$ and then show our predictions for the $\Lambda\bar{\Lambda}$ invariant mass spectra measured in the reactions $e^+e^- \rightarrow \eta\Lambda\bar{\Lambda}$ and $e^+e^- \rightarrow \phi\Lambda\bar{\Lambda}$. We also discuss the situation for $\psi(3868) \rightarrow \eta\Lambda\bar{\Lambda}$ and $\gamma p \rightarrow p\Lambda\bar{\Lambda}$. The paper closes with a short summary. The appendix contains a brief discussion of the $\Lambda\bar{\Lambda}$ correlations measured by ALICE.

2 Treatment of the $\Lambda\bar{\Lambda}$ final-state interaction

Our calculation of the $\Lambda\bar{\Lambda}$ invariant-mass spectrum is based on the distorted wave Born approximation (DWBA), where the reaction amplitude A is given schematically by [43, 44]

$$A = A^0 + A^0 G^{\Lambda\bar{\Lambda}} T^{\Lambda\bar{\Lambda}}. \quad (1)$$

Here, A^0 is the elementary (or primary) production amplitude, $G^{\Lambda\bar{\Lambda}}$ the free $\Lambda\bar{\Lambda}$ Green's function, and $T^{\Lambda\bar{\Lambda}}$ the $\Lambda\bar{\Lambda}$ reaction amplitude. For a particular (uncoupled) $\Lambda\bar{\Lambda}$ partial wave with orbital angular momentum L Eq. (1) reads

$$A_L = A_L^0 + \int_0^\infty \frac{dpp^2}{(2\pi)^3} A_L^0 \frac{1}{2E_k - 2E_p + i0^+} T_L(p, k; E_k), \quad (2)$$

where T_L denotes the partial-wave projected T -matrix, and k and E_k are the momentum and energy of the Λ (or $\bar{\Lambda}$) in the center-of-mass system of the $\Lambda\bar{\Lambda}$ pair. The quantity $T_L(p, k; E_k)$ is obtained by solving the Lippmann-Schwinger (LS) equation,

$$T_L(p', k; E_k) = V_L(p', k) + \int_0^\infty \frac{dpp^2}{(2\pi)^3} V_L(p', p) \frac{1}{2E_k - 2E_p + i0^+} T_L(p, k; E_k), \quad (3)$$

for a specific $\Lambda\bar{\Lambda}$ potential V_L . In the case of coupled partial waves like the 3S_1 – 3D_1 the corresponding coupled LS equation is solved [45], and then T_{LL} is used in Eq. (2).

In principle, the elementary production amplitude A_L^0 in Eq. (2) depends on the total energy and also on the $\Lambda\bar{\Lambda}$ momentum and the momentum of the additional particle relative to the $\Lambda\bar{\Lambda}$ system [46]. In the near-threshold region $A_L^0 = \bar{A}_L^0 k^L$. The variation of \bar{A}_L^0 with regard to the other variables should be rather small as compared to the strong momentum dependence induced by the $\Lambda\bar{\Lambda}$ FSI. Therefore, we neglect it in the following so that Eq. (2) reduces to

$$A_L = \bar{A}_L^0 k^L \times \left[1 + \int_0^\infty \frac{dpp^2}{(2\pi)^3} \frac{p^L}{k^L} \frac{1}{2E_k - 2E_p + i0^+} T_L(p, k; E_k) \right]. \quad (4)$$

with \bar{A}_L^0 a constant. We found, however, that a straight and simplistic off-shell extension $\bar{A}_L^0 k^L \rightarrow \bar{A}_L^0 p^L$ in the integral in Eq. (4) leads to a strong and seemingly artificial enhancement of the principal-value part for P -waves, see also the discussion in Ref. [47]. Therefore, in order to avoid this artifact we attenuate the P -wave momentum factor $p(k)$ by replacing it with $p \exp(-p^2/\Lambda^2)$

(and likewise for k) in the actual calculation. The considered value for Λ (500 \sim 600 MeV/c) are chosen in line with our experience in studying FSI effects with chiral $N\bar{N}$ potentials [44] where the cutoff of the intrinsic regulator is of that order. Note that $k \simeq \Lambda \simeq 500$ MeV/c corresponds to an invariant mass of roughly 2.45 GeV. Thus, with such a value the on-shell properties of the $\Lambda\bar{\Lambda}$ amplitude in the region near the $\Lambda\bar{\Lambda}$ threshold we are interested in remain practically unmodified. For a thorough discussion of various aspects of the treatment of FSI effects, see Refs. [46, 48, 49] and also [50].

The $\Lambda\bar{\Lambda}$ invariant-mass spectrum is calculated via

$$\frac{d\sigma}{dM(\Lambda\bar{\Lambda})} \propto k |A_L(k)|^2, \quad (5)$$

which is valid when the (total) energy is significantly larger than the $\phi\Lambda\bar{\Lambda}$ or $\eta\Lambda\bar{\Lambda}$ threshold energies. Then for low $\Lambda\bar{\Lambda}$ invariant masses the relative momentum of the third particle is large and it does not distort the signal of interest. This condition is well fulfilled by the BESIII measurements.

In the present calculations we employ $\Lambda\bar{\Lambda}$ potentials which were established within the Jülich meson-baryon model in studies of the reaction $p\bar{p} \rightarrow \Lambda\bar{\Lambda}$ [39–42]. In those works the hyperon-production reaction is considered within a coupled-channel approach, which allowed to take into account rigorously the effects of the initial ($p\bar{p}$) and final ($\Lambda\bar{\Lambda}$) state interactions. Both play a role for describing the data for energies near the production threshold. For details of the potentials we refer the reader to the cited works. Here we just want to mention that the elastic parts of the interactions in the $p\bar{p}$ and $\Lambda\bar{\Lambda}$ channels are described by meson exchanges, whereas annihilation processes are accounted for by phenomenological optical potentials.

We consider a variety of potentials in order to assess a possible (and unavoidable) model dependence of the results. Specifically, we use the $\Lambda\bar{\Lambda}$ potentials I, II, and III of Ref. [39] (cf. Table III) and “K” from Ref. [41] (Table II), denoted by IV below. The models differ by variations in the employed parameterization of the $N\bar{N}$ annihilation potential and by differences in the $p\bar{p} \rightarrow \Lambda\bar{\Lambda}$ transition mechanism. All of them provide a rather good overall description of the wealth of $p\bar{p} \rightarrow \Lambda\bar{\Lambda}$ data collected by the P185 Collaboration [1]. In particular, the total reaction cross sections produced by those potentials agree with each other and with the experiment up to $p_{\text{lab}} \approx 1700$ MeV/c (corresponding to $\sqrt{s} \approx 2.32$ GeV or an excess energy $Q = \sqrt{s} - 2m_\Lambda$ of about 90 MeV). Even spin-dependent observables (analyzing powers, spin-correlation parameters) are, in general, described fairly well. For reference, in the appendix

the scattering lengths of those potentials are summarized and a brief discussion of results for the $\Lambda\bar{\Lambda}$ correlations measured by the ALICE Collaboration [21] is provided. Finally, we emphasize again that the validity of treating FSI effects via Eqs. (4) and (5) is clearly limited, say to excess energies of 50 to 100 MeV. With increasing invariant mass the momentum dependence of the reaction/production mechanism should become more and more relevant and will likewise influence the invariant-mass spectrum. Last but not least when approaching the $\Sigma\bar{\Sigma}$ threshold the overall dynamics could change significantly [28].

3 Results

In the following we present predictions for the $\Lambda\bar{\Lambda}$ invariant-mass spectrum for the reactions $e^+e^- \rightarrow \eta\Lambda\bar{\Lambda}$ and $e^+e^- \rightarrow \phi\Lambda\bar{\Lambda}$. The former is interesting because it involves the same $\Lambda\bar{\Lambda}$ state (FSI) as $e^+e^- \rightarrow \Lambda\bar{\Lambda}$. In the latter case FSI effects in $\Lambda\bar{\Lambda}$ P -waves are expected to play a role, considering the helicity-angle analysis of the BESIII data [18]. As mentioned above, the calculations utilize $\Lambda\bar{\Lambda}$ potentials from [39, 41] which have been already explored in our study of the electromagnetic form factors of the Λ in the time-like region [28].

3.1 The reaction $e^+e^- \rightarrow \eta\Lambda\bar{\Lambda}$

We start with reminding the reader on the situation for $e^+e^- \rightarrow \Lambda\bar{\Lambda}$. Experimental results in the near-threshold region are presented in Fig. 1 (bottom), together with our predictions based on various $\Lambda\bar{\Lambda}$ potentials [28, 34]. One can see on the one hand that all interactions yield a more or less flat behavior of the cross section, in line with the BaBar data [13]. On the other hand, the data point from BESIII [15] at 2232.4 MeV, i.e. just about 1 MeV above the $\Lambda\bar{\Lambda}$ threshold at $2m_\Lambda = 2231.4$ MeV, deviates from the overall trend and is not reproduced by our calculation. As demonstrated in works by others, that data point can be only described by introducing a narrow and so far unknown resonance located very near the threshold ($M_x = 2230.9$ MeV, $\Gamma_x = 4.7$ MeV) [35] or by a suitably adjusted contribution of the sub-threshold resonance $\phi(2170)$ in combination with an additional resonance at 2340 MeV [30].

Interestingly, initial data for $p\bar{p} \rightarrow \Lambda\bar{\Lambda}$ provided some support for a near-threshold resonance in the 3S_1 $\Lambda\bar{\Lambda}$ state [51]. However, a later high-statistics measurement by Barnes et al. [5] ruled that out. In fact, including a narrow near-threshold resonance in our $\Lambda\bar{\Lambda}$ potentials would completely spoil the agreement with the

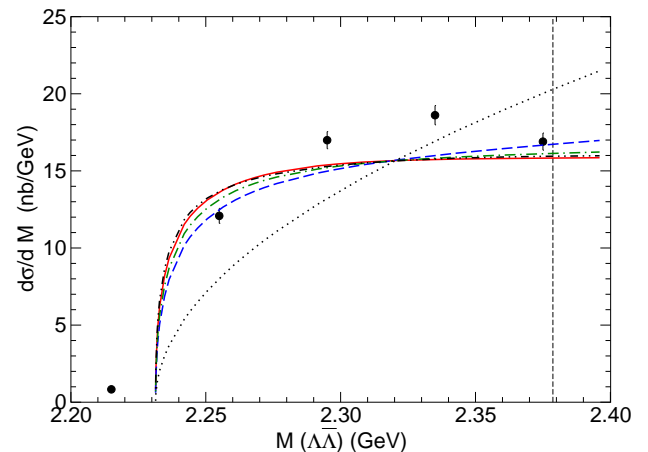
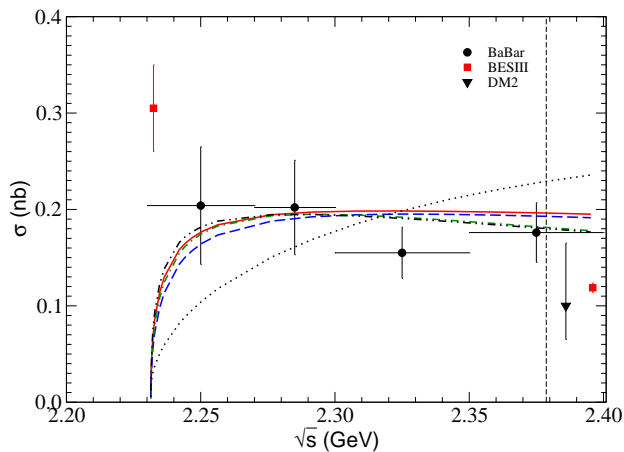
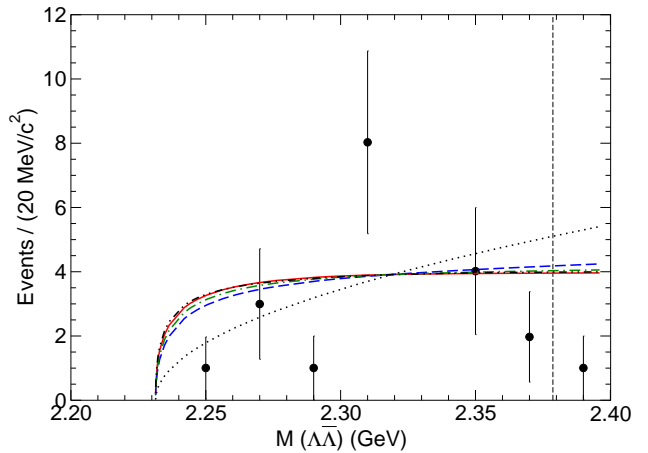
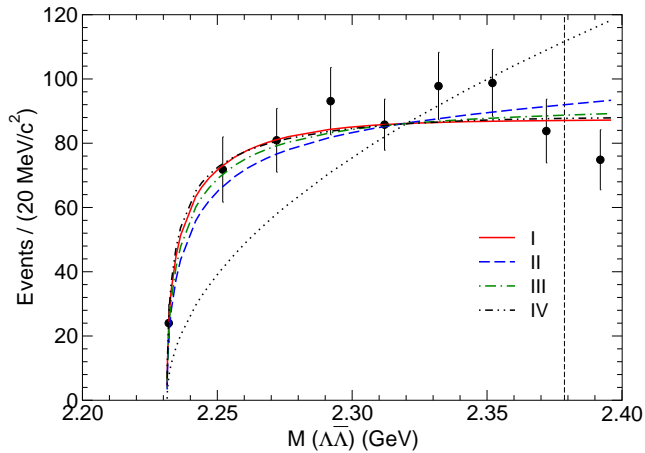


Fig. 1 Top: Results for $e^+e^- \rightarrow \eta\Lambda\bar{\Lambda}$ based on the 3S_1 partial wave of the $\Lambda\bar{\Lambda}$ models I-IV [39, 41]. Data are from Ref. [19]. The phase space behavior is indicated by the dotted line. The vertical thin dash-dotted line marks the $\Sigma^+\Sigma^+$ threshold which is around 2.379 GeV. All curves are arbitrarily normalized so that they coincide at $\sqrt{s} \approx 2.32$ GeV. Bottom: Corresponding results for $e^+e^- \rightarrow \Lambda\bar{\Lambda}$, see Refs. [28, 34]. Data are from Refs. [12] (DM2), [13] (BaBar), and [15] (BESIII).

$p\bar{p} \rightarrow \Lambda\bar{\Lambda}$ data. It should be mentioned that a partial-wave analysis of the reaction $p\bar{p} \rightarrow \Lambda\bar{\Lambda}$, performed by Bugg [52] indicated again the presence of a resonance. However, its width is very large ($\Gamma \approx 275$ MeV). In our opinion that resonance has to be considered simply as an effective parameterization of the FSI effects in the 3S_1 - 3D_1 partial wave rather than as indication for a physical state.

The new measurement of the $\Lambda\bar{\Lambda}$ mass spectrum in the reaction $e^+e^- \rightarrow \eta\Lambda\bar{\Lambda}$ is shown in Fig. 1 (top). The possible $\Lambda\bar{\Lambda}$ states near threshold are 3S_1 (1^{--}) and 1P_1 (1^{+-}), where the former is the partial wave which also causes the enhancement in the $e^+e^- \rightarrow \Lambda\bar{\Lambda}$ cross

Fig. 2 Invariant-mass spectra for $\psi(3686) \rightarrow \eta\Lambda\bar{\Lambda}$ from the BESIII Collaboration [10] (top) and preliminary results for $\gamma p \rightarrow p\Lambda\bar{\Lambda}$ from GlueX [23] (bottom). Same description of curves as in Fig 1.

section. Indeed, the invariant-mass spectrum calculated via Eq. (5), including FSI effects from our $\Lambda\bar{\Lambda}$ potentials in the 3S_1 partial wave, describes the BESIII data strikingly well over the whole considered invariant-mass region. Note specifically the one data point very close to threshold which is exactly in line with the energy dependence generated by the FSI. In view of that, it is hard to believe that something unusual happens only in $e^+e^- \rightarrow \Lambda\bar{\Lambda}$ at the threshold whereas for other reactions a consistent and convincing description of the experiments is achieved by the FSI in the same $\Lambda\bar{\Lambda}$ partial wave.

In Fig. 2 we show result for two other reactions where the $\Lambda\bar{\Lambda}$ invariant-mass spectrum has been measured. Also in those cases we expect that the 3S_1 partial wave provides the dominant FSI effect. Unfortunately,

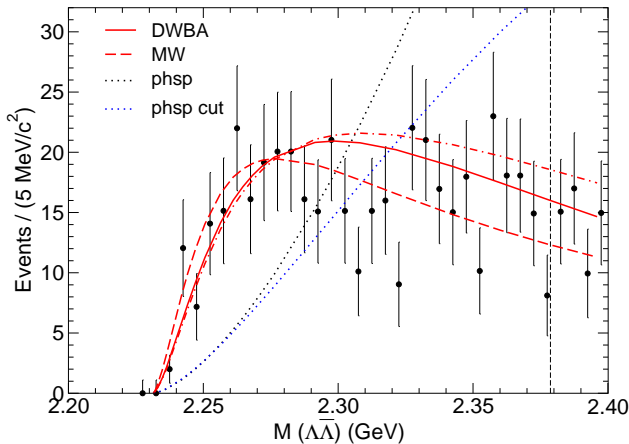


Fig. 3 Invariant-mass spectrum for $e^+e^- \rightarrow \phi\Lambda\bar{\Lambda}$. The results are based on the 3P_2 partial wave of the $\Lambda\bar{\Lambda}$ model I [39]. The curves correspond to the DWBA calculation (with cutoff 500 (solid) and 600 MeV (dash-dotted) and the Migdal-Watson approximation (dashed), see text. The P -wave phase space (k^3), without (phsp) and with cutoff (phsp cut), is indicated by the dotted lines. Data are from Ref. [18].

the statistics of the BESIII data on $\psi(3686) \rightarrow \eta\Lambda\bar{\Lambda}$ (top) is too low for allowing reliable conclusions. The invariant-mass spectrum from a measurement of the reaction $\gamma p \rightarrow p\Lambda\bar{\Lambda}$ by GlueX is roughly in line with our prediction based on the FSI by the 3S_1 partial wave, but we want to emphasize that those data are still preliminary. Moreover, for that reaction there are no strict selection rules so that the 1S_0 partial wave can likewise contribute and FSI effects there could have an impact on the result, too.

3.2 The reaction $e^+e^- \rightarrow \phi\Lambda\bar{\Lambda}$

Recently, the BESIII Collaboration [18] has also published data for the reaction $e^+e^- \rightarrow \phi\Lambda\bar{\Lambda}$ [18]. The measurement is characterized by an excellent momentum resolution and by the fact that the angular distributions have been measured and analysed. According to that analysis the $\Lambda\bar{\Lambda}$ pair is produced in the 1^{++} , 2^{++} , or 2^{-+} states, i.e. in the $\Lambda\bar{\Lambda}$ partial waves 3P_1 , 3P_2 , or 1D_2 . For illustration, in the following we will show results for all triplet P -waves (3P_0 , 3P_1 , 3P_2) of the $\Lambda\bar{\Lambda}$ potentials.

However, first we focus on aspects of the treatment of P -wave interactions in our FSI formalism. As already mentioned in Sect. 2, in the case of P -wave interactions we include a cutoff in the evaluation within the DWBA (4). In Fig. 3 we examine the effect of this treatment. The (upper) dotted line represents the phase-

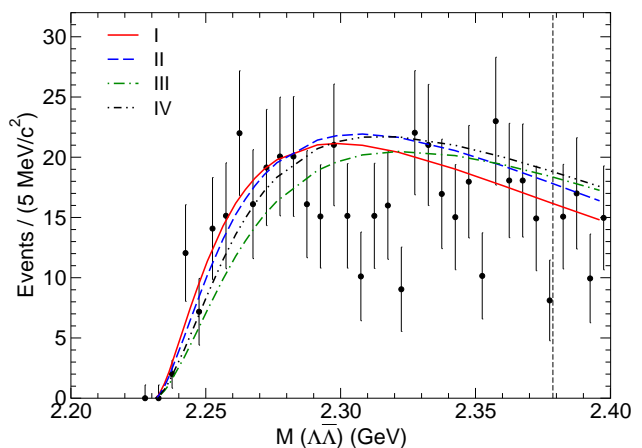
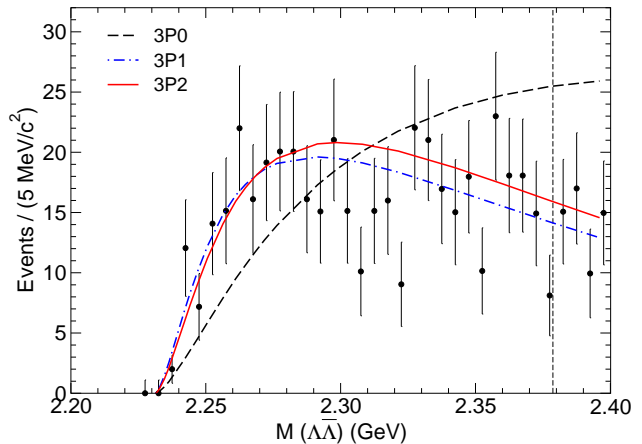


Fig. 4 Invariant-mass spectrum for $e^+e^- \rightarrow \phi\Lambda\bar{\Lambda}$. Top: Results for different $\Lambda\bar{\Lambda}$ partial waves (3P_0 , 3P_1 , 3P_2) based on $\Lambda\bar{\Lambda}$ model I [39]. Bottom: Results for different $\Lambda\bar{\Lambda}$ models I, II, III [39], and IV [41], based on the 3P_2 partial wave. Data are from Ref. [18].

space behavior of a P -wave, where the invariant-mass spectrum is then proportional to k^3 . In case of the blue (lower) dotted line the cutoff factor is multiplied. One can see that the change is only small to moderate over the interesting region of say $M(\Lambda\bar{\Lambda}) \lesssim 2.32$ GeV. Specifically, no additional and undesirable energy dependence is introduced. The effect of the FSI, calculated via Eq. (4), leads to a drastic modification of the spectrum, visualized here for the 3P_2 partial wave of model I. For illustration we show predictions based on a cutoff of 500 MeV (solid line) and for 600 MeV (dash-dotted line), and also results obtained within the so-called Migdal-Watson (MW) approximation (dashed line) where the invariant-mass spectrum is basically

given by $T_L(k, k; E_k)/k$ [47]. One can see that all the results are qualitatively similar.

Predictions for the invariant-mass spectrum based on the 3P_0 , 3P_1 , and 3P_2 partial waves of the $\Lambda\bar{\Lambda}$ potential I are shown in Fig. 4 (top). Here 500 MeV is used for the cutoff. Obviously, the result for the 3P_1 as well as those for the 3P_2 are well in line with the experiment. Those two states were also favored by the helicity-angle analysis of BESIII [18]. For the 3P_0 partial wave, which anyway is practically excluded by that analysis, the FSI effects would fall short to describe the data. In order to complete the picture, in Fig. 4 (bottom) we show results based on all $\Lambda\bar{\Lambda}$ potentials I-IV, selectively for the 3P_2 partial wave. Obviously, the model-dependence of the predictions is quite small, something we already observed above when considering FSI effects due to the 3S_1 state.

The invariant-mass spectrum for $e^+e^- \rightarrow \phi\Lambda\bar{\Lambda}$ was also studied by Milstein and Salnikov [53] and they too achieved agreement with the data by including FSI effects. They also showed that with the 1D_2 partial wave (i.e. the 2^{-+} state) one cannot describe the near-threshold behavior and, therefore, we did not consider this state in our calculations. Anyway, we want to emphasize that in their investigation the potential was specifically constructed for and fitted to the BESIII data. As said above, the $\Lambda\bar{\Lambda}$ potentials employed by us were established in a study of the $p\bar{p} \rightarrow \Lambda\bar{\Lambda}$ reaction and fitted to the LEAR data. Thus our result for the $\Lambda\bar{\Lambda}$ invariant-mass spectrum are in fact predictions. We note that our potentials are also more realistic because they include effects from $\Lambda\bar{\Lambda}$ annihilation [39].

4 Summary

In the present work we have investigated invariant-mass spectra for the reactions $e^+e^- \rightarrow \eta\Lambda\bar{\Lambda}$ and $e^+e^- \rightarrow \phi\Lambda\bar{\Lambda}$ close to the $\Lambda\bar{\Lambda}$ threshold. Specific emphasis has been put on the role played by the interaction in the final $\Lambda\bar{\Lambda}$ system which is taken into account rigorously. For it a variety of $\Lambda\bar{\Lambda}$ potential models have been employed that have been established in the analysis of data on the reaction $p\bar{p} \rightarrow \Lambda\bar{\Lambda}$ from the LEAR facility at CERN.

It turned out that the near-threshold invariant-mass dependence of the $\Lambda\bar{\Lambda}$ spectra observed in those two reactions can be well reproduced by considering the $\Lambda\bar{\Lambda}$ FSI in the partial waves suggested by the helicity-angle analysis of the experiment. In the case of $e^+e^- \rightarrow \eta\Lambda\bar{\Lambda}$ the partial wave responsible for the FSI (3S_1) is identical to the one which dominates the $e^+e^- \rightarrow \Lambda\bar{\Lambda}$ cross section near threshold. It is shown that the enhancement generated by the FSI in this state allows one to

achieve a consistent description of both reactions. However, a nonzero “threshold” cross section as suggested for the latter reaction in the BESIII experiment [15] is not observed in the new $\eta\Lambda\bar{\Lambda}$ data. In fact, none of the reactions with $\Lambda\bar{\Lambda}$ in the final state, measured in recent times, confirms or supports the existence of a narrow near-threshold resonance that couples to the $\Lambda\bar{\Lambda}$ system.

Acknowledgements: Work supported by the European Research Council (ERC) under the European Union’s Horizon 2020 research and innovation programme (grant no. 101018170, EXOTIC), and by the DFG and the NSFC through funds provided to the Sino-German CRC 110 “Symmetries and the Emergence of Structure in QCD” (Project number 196253076 - TRR 110). The work of UGM was also supported by the Chinese Academy of Sciences (CAS) through a President’s International Fellowship Initiative (PIFI) (Grant No. 2018DM0034) and by the VolkswagenStiftung (Grant No. 93562).

Appendix A: Predictions for the $\Lambda\bar{\Lambda}$ correlation function

For completeness, in Table 2 we summarize the scattering lengths for the employed $\Lambda\bar{\Lambda}$ potentials.

Table 2 $\Lambda\bar{\Lambda}$ scattering lengths (in fm) in the 1S_0 and 3S_1 partial waves of the employed $\Lambda\bar{\Lambda}$ potentials [39, 41]. The spin-averaged value by the ALICE Collaboration is from an analysis of the $\Lambda\bar{\Lambda}$ correlation function measured in Pb-Pb collisions [20].

potential	$a({}^1S_0)$	$a({}^3S_1)$
I	0.32 – i0.52	0.74 – i0.56
II	0.67 – i1.14	0.66 – i0.37
III	1.42 – i1.15	1.00 – i0.44
IV	1.56 – i1.40	0.98 – i0.65
ALICE	(0.90 ± 0.16) – i(0.40 ± 0.18)	

Furthermore, for illustration we provide predictions for the two-particle momentum correlation function in comparison to data of the ALICE Collaboration from pp collisions at $\sqrt{s} = 13$ TeV [21], see Fig. 5. We want to emphasize that these results are only meant for providing a qualitative impression. The calculations were performed with the wave functions in the 1S_0 and 3S_1 partial waves in the standard way, assuming a Gaussian function for the source [54–56]. However, possible contributions from higher partial waves and from

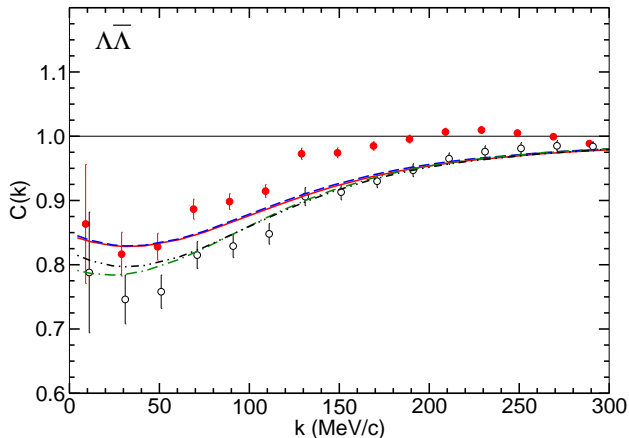


Fig. 5 $\Lambda\bar{\Lambda}$ correlation function measured in pp collisions at 13 TeV by the ALICE Collaboration [21]. Filled symbols are the original data while the opaque symbols include corrections for the background as estimated in that work. The calculation is based on the $\Lambda\bar{\Lambda}$ wave functions in the 1S_0 and 3S_1 partial waves, see text. Same description of curves as in Fig. 1.

the annihilation channels were omitted, see [21, 55] for more details. In addition, no adjustment of femtoscopic parameters, like the source radius R and the so-called feed-down parameter λ [54], was done. Here we simply chose values ($R = 1.1$ fm, $\lambda = 0.35$) comparable to those suggested in [21]. Nonetheless, one can see that there is a good qualitative agreement with the measurement for all the four potentials. Remarkably, the moderate rise of the correlation function at very low momenta indicated by the data is reproduced by the calculations. In any case, there is no indication for a near-threshold resonance.

References

1. E. Klempt, F. Bradamante, A. Martin and J. M. Richard, Phys. Rept. **368**, 119 (2002).
2. P. D. Barnes *et al.*, Phys. Lett. B **229**, 432 (1989).
3. P. D. Barnes *et al.*, Nucl. Phys. A **526**, 575 (1991).
4. P. D. Barnes *et al.*, Phys. Rev. C **54**, 1877 (1996).
5. P. D. Barnes *et al.*, Phys. Rev. C **62**, 055203 (2000).
6. K. D. Paschke *et al.*, Phys. Rev. C **74**, 015206 (2006).
7. Y. W. Chang *et al.* [Belle], Phys. Rev. D **79**, 052006 (2009).
8. J. P. Lees *et al.* [BaBar], Phys. Rev. D **89**, 112002 (2014).
9. M. Ablikim *et al.* [BESIII], Phys. Rev. D **87**, 052007 (2013).
10. M. Ablikim *et al.* [BESIII], Phys. Rev. D **106**, 072006 (2022).
11. M. Ablikim *et al.* [BESIII], Phys. Rev. D **106**, 112011 (2022).
12. D. Bisello *et al.* [DM2 Collaboration], Z. Phys. C **48**, 23 (1990).
13. B. Aubert *et al.* [BaBar Collaboration], Phys. Rev. D **76**, 092006 (2007).
14. S. Dobbs, A. Tomaradze, T. Xiao, K. K. Seth and G. Bonvicini, Phys. Lett. B **739**, 90 (2014).
15. M. Ablikim *et al.* [BESIII], Phys. Rev. D **97**, 032013 (2018).
16. M. Ablikim *et al.* [BESIII], Phys. Rev. Lett. **123**, 122003 (2019).
17. M. Ablikim *et al.* [BESIII], Phys. Rev. D **104**, L091104 (2021).
18. M. Ablikim *et al.* [BESIII], Phys. Rev. D **104**, 052006 (2021).
19. M. Ablikim *et al.* [BESIII], [arXiv:2211.10755 [hep-ex]].
20. S. Acharya *et al.* [ALICE], Phys. Lett. B **802**, 135223 (2020).
21. S. Acharya *et al.* [ALICE], Phys. Lett. B **829**, 137060 (2022).
22. H. Li *et al.* [GlueX], AIP Conf. Proc. **2249**, 030037 (2020).
23. P. Pauli [GlueX], EPJ Web Conf. **271**, 02001 (2022).
24. X. Zhou, L. Yan, R. B. Ferroli and G. Huang, Symmetry **14**, 144 (2022).
25. K. Schönning, V. Batozskaya, P. Adlarson and X. Zhou, [arXiv:2302.13071 [hep-ph]].
26. R. Baldini, S. Pacetti, A. Zallo and A. Zichichi, Eur. Phys. J. A **39**, 315 (2009).
27. O. D. Dalkarov, P. A. Khakhulin and A. Y. Voronin, Nucl. Phys. A **833**, 104 (2010).
28. J. Haidenbauer and U.-G. Meißner, Phys. Lett. B **761**, 456 (2016).
29. Y. Yang and Z. Lu, Mod. Phys. Lett. A **33**, 1850133 (2018).
30. X. Cao, J.-P. Dai and Y.-P. Xie, Phys. Rev. D **98**, 094006 (2018).
31. Y. Yang, D.-Y. Chen and Z. Lu, Phys. Rev. D **100**, 073007 (2019).
32. L.-Y. Xiao, X.-Z. Weng, X.-H. Zhong and S.-L. Zhu, Chin. Phys. C **43**, 113105 (2019).
33. G. Ramalho, M. T. Peña and K. Tsushima, Phys. Rev. D **101**, 014014 (2020).
34. J. Haidenbauer, U.-G. Meißner and L. Y. Dai, Phys. Rev. D **103**, 014028 (2021).
35. Z. Y. Li, A. X. Dai and J. J. Xie, Chin. Phys. Lett. **39**, 011201 (2022).

-
36. Y. H. Lin, H.-W. Hammer and U.-G. Meißner, Eur. Phys. J. C **82**, 1091 (2022).
 37. Y. M. Bystritskiy and A. I. Ahmadov, Phys. Rev. D **105**, 116012 (2022).
 38. E. Tomasi-Gustafsson and S. Pacetti, Phys. Rev. C **106**, 035203 (2022).
 39. J. Haidenbauer, T. Hippchen, K. Holinde, B. Holzenkamp, V. Mull and J. Speth, Phys. Rev. C **45**, 931 (1992).
 40. J. Haidenbauer, K. Holinde, V. Mull and J. Speth, Phys. Lett. B **291**, 223 (1992).
 41. J. Haidenbauer, K. Holinde, V. Mull and J. Speth, Phys. Rev. C **46**, 2158 (1992).
 42. J. Haidenbauer, K. Holinde and J. Speth, Nucl. Phys. A **562**, 317 (1993).
 43. A. Sibirtsev, J. Haidenbauer, S. Krewald, U.-G. Meißner and A. W. Thomas, Phys. Rev. D **71**, 054010 (2005).
 44. X. W. Kang, J. Haidenbauer and U.-G. Meißner, Phys. Rev. D **91**, 074003 (2015).
 45. J. Haidenbauer, X. W. Kang and U.-G. Meißner, Nucl. Phys. A **929**, 102 (2014).
 46. A. Gasparyan, J. Haidenbauer and C. Hanhart, Phys. Rev. C **72**, 034006 (2005).
 47. D. R. Entem and F. Fernandez, Phys. Rev. D **75**, 014004 (2007).
 48. C. Hanhart and K. Nakayama, Phys. Lett. B **454**, 176 (1999).
 49. V. Baru, A. M. Gasparian, J. Haidenbauer, A. E. Kudryavtsev and J. Speth, Phys. Atom. Nucl. **64**, 579 (2001) [Yad. Fiz. **64**, 633 (2001)].
 50. M. L. Goldberger and K. M. Watson, *Collision Theory* (John Wiley and Sons, New York 1964), Chap. 9.3.
 51. J. Carbonell, K. V. Protasov and O. D. Dalkarov, Phys. Lett. B **306**, 407 (1993).
 52. D. V. Bugg, Eur. Phys. J. C **36**, 161 (2004).
 53. A. I. Milstein and S. G. Salnikov, Phys. Rev. D **105**, L031501 (2022).
 54. S. Cho *et al.* [ExHIC Collaboration], Prog. Part. Nucl. Phys. **95**, 279 (2017).
 55. J. Haidenbauer, Nucl. Phys. A **981**, 1 (2019).
 56. J. Haidenbauer and U.-G. Meißner, Phys. Lett. B **829**, 137074 (2022).